Carrier density dependence of plasmon-enhanced nonradiative energy transfer in a hybrid quantum well-quantum dot structure

L.J. Higgins[1,*], V.D. Karanikolas[1], C.A. Marocico[1], A.P. Bell[1], T. C. Sadler[2], P.J. Parbrook[2] and A.L. Bradley[1]

[1]Department of Physics and CRANN, Trinity College Dublin, College Green, Dublin 2, Ireland
[2]Tyndall National Institute and School of Engineering, University College Cork, Lee Maltings, Prospect Row, Cork, Ireland
**higginlu@tcd.ie*

Abstract: An array of Ag nanoboxes fabricated by helium-ion lithography is used to demonstrate plasmon-enhanced nonradiative energy transfer in a hybrid quantum well-quantum dot structure. The nonradiative energy transfer, from an InGaN/GaN quantum well to CdSe/ZnS nanocrystal quantum dots embedded in an ~80 nm layer of PMMA, is investigated over a range of carrier densities within the quantum well. The plasmon-enhanced energy transfer efficiency is found to be independent of the carrier density, with an efficiency of 25% reported. The dependence on carrier density is observed to be the same as for conventional nonradiative energy transfer. The plasmon-coupled energy transfer enhances the QD emission by 58%. However, due to photoluminescence quenching effects an overall increase in the QD emission of 16% is observed.

OCIS codes: (250.5403) Plasmonics; (230.0250) Optoelectronics; (250.5230) Photoluminescence; (250.5590) Quantum-well, -wire and -dot devices.

References and links

1. E. F. Schubert, *Light-Emitting Diodes* (Cambridge University, 2006).
2. H. V. Demir, S. Nizamoglu, T. Erdem, E. Mutlugun, N. Gaponik, and A. Eychmuller, "Quantum dot integrated LEDs using photonic and excitonic color conversion," Nano Today **6**(6), 632–647 (2011).
3. H. S. Chen, C.-K. Hsu, and H. Y. Hong, "InGaN-CdSe-ZnSe quantum dots white LEDs," IEEE Photon. Technol. Lett. **18**(1), 193–195 (2006).
4. M. Achermann, M. A. Petruska, S. Kos, D. L. Smith, D. D. Koleske, and V. I. Klimov, "Energy-transfer pumping of semiconductor nanocrystals using an epitaxial quantum well," Nature **429**(6992), 642–646 (2004).
5. S. Nizamoglu, E. Sari, J. H. Baek, I. H. Lee, and H. V. Demir, "White light generation by resonant nonradiative energy transfer from epitaxial InGaN/GaN quantum wells to colloidal CdSe/ZnS core/shell quantum dots," New J. Phys. **10**(12), 123001 (2008).
6. T. Förster, "Intermolecular energy migration and fluorescence," Ann. Phys. **437**, 55–75 (1948).
7. M. Achermann, M. A. Petruska, D. D. Koleske, M. H. Crawford, and V. I. Klimov, "Nanocrystal-based light-emitting diodes utilizing high-efficiency nonradiative energy transfer for color conversion," Nano Lett. **6**(7), 1396–1400 (2006).
8. A. J. Shaw, A. L. Bradley, J. F. Donegan, and J. G. Lunney, "GaN resonant cavity light-emitting diodes for plastic optical fiber applications," IEEE Photon. Technol. Lett. **16**(9), 2006–2008 (2004).
9. T. Fugii, Y. Gao, R. Sharma, E. L. Hu, S. P. Denbaars, and S. Nakamura, "Increase in the extraction efficiency of GaN-based light emitting diodes via surface roughening," Appl. Phys. Lett. **84**(6), 855 (2004).
10. S. Chanyawadee, P. G. Lagoudakis, R. T. Harley, M. D. B. Charlton, D. V. Talapin, H. W. Huang, and C. H. Lin, "Increased color-conversion efficiency in hybrid light-emitting diodes utilizing non-radiative energy transfer," Adv. Mater. **22**(5), 602–606 (2010).
11. B. Guzelturk, S. Nizamoglu, D. Jeon, I. Lee and H. V. Demir, "Strong nonradiative energy transfer from the nanopillars of quantum wells to quantum dots: efficient excitonic color conversion for light emitting diodes," in proceedings of CLEO, pp. 1–2 (2012).
12. D. Basko, G. C. La Rocca, F. Bassini, and V. M. Agranovich, "Förster energy transfer from a semiconductor quantum well to an organic material overlayer," Eur. Phys. J. B **8**(3), 353–362 (1999).

#228319 - $15.00 USD Received 20 Nov 2014; revised 19 Dec 2014; accepted 25 Dec 2014; published 20 Jan 2015

13. G. Itskos, G. Heliotis, P. G. Lagoudakis, J. Lupton, N. P. Barradas, E. Alves, S. Pereira, I. M. Watson, M. D. Dawson, J. Feldmann, R. Murray, and D. D. C. Bradley, "Efficient dipole-dipole coupling of Mott-Wannier and Frenkel excitons in (Ga,In)N quantum well/polyfluorene semiconductor hetero structures," Phys. Rev. B **76**(3), 035344 (2007).
14. C. R. Belton, G. Itskos, G. Heliotis, P. N. Stavrinou, P. G. Lagoudakis, J. Lupton, S. Pereira, E. Gu, C. Griffin, B. Guillabert, I. M. Watson, A. R. Mackintosh, R. A. Pethrick, J. Feldmann, R. Murray, M. D. Dawson, and D. D. C. Bradley, "New light from hybrid inorganic-organic emitters," J. Phys. D Appl. Phys. **41**(9), 094006 (2008).
15. G. Itskos, C. R. Belton, G. Heliotis, I. M. Watson, M. D. Dawson, R. Murray, and D. D. C. Bradley, "White light emission via cascade Förster energy transfer in (Ga, In)N quantum well/polymer blend hybrid structures," Nanotechnology **20**(27), 275207 (2009).
16. G. Heliotis, G. Itskos, R. Murray, M. D. Dawson, I. M. Watson, and D. D. C. Bradley, "Hybrid inorganic/organic semiconductor heterostructures with efficient non-radiative energy transfer," Adv. Mater. **18**(3), 334–338 (2006).
17. R. Smith, B. Liu, J. Bai, and T. Wang, "Hybrid III-nitride/organic semiconductor nanostructure with high efficiency nonradiative energy transfer for white light emitters," Nano Lett. **13**(7), 3042–3047 (2013).
18. A. Neogi, C. W. Lee, H. O. Everitt, T. Kuroda, A. Tackeuchi, and E. Yablonovitch, "Enhancement of spontaneous recombination rate in a quantum well by resonant surface plasmon coupling," Phys. Rev. B **66**(15), 153305 (2002).
19. K. Okamoto, I. Niki, A. Shvartser, Y. Narukawa, T. Mukai, and A. Scherer, "Surface-plasmon-enhanced light emitters based on InGaN quantum wells," Nat. Mater. **3**(9), 601–605 (2004).
20. J. Henson, E. Dimakis, J. DiMaria, R. Li, S. Minissale, L. Dal Negro, T. D. Moustakas, and R. Paiella, "Enhanced near-green light emission from InGaN quantum wells by use of tunable plasmonic resonances in silver nanoparticle arrays," Opt. Express **18**(20), 21322–21329 (2010).
21. G. Lozano, D. J. Louwers, S. R. K. Rodriguez, S. Murai, O. T. A. Jansen, M. A. Verschuuren, and J. G. Rivas, "Plasmonics for solid-state lighting: enhanced excitation and directional emission of highly efficient light sources," Light: Science and Applications **2**(5), e66 (2013).
22. M. K. Kwon, J. Y. Kim, B. H. Kim, I. K. Park, C. Y. Cho, C. C. Byeon, and S. J. Park, "Surface-plasmon enhanced light-emitting diodes," Adv. Mater. **20**(7), 1253–1257 (2008).
23. P. P. Pompa, L. Martiradonna, A. D. Torre, F. D. Sala, L. Manna, M. De Vittorio, F. Calabi, R. Cingolani, and R. Rinaldi, "Metal-enhanced fluorescence of colloidal nanocrystals with nanoscale control," Nat. Nanotechnol. **1**(2), 126–130 (2006).
24. K. Tanaka, E. Plum, J. Y. Ou, T. Uchino, and N. I. Zheludev, "Multifold enhancement of quantum dot luminescence in plasmonic metamaterials," Phys. Rev. Lett. **105**(22), 227403 (2010).
25. V. K. Komarala, Y. P. Rakovich, A. L. Bradley, S. J. Byrne, Y. K. Gun'ko, N. Gaponik, and A. Eychmüller, "Off-resonance surface plasmon enhanced spontaneous emission from CdTe quantum dots," Appl. Phys. Lett. **89**(25), 253118 (2006).
26. J. Zhang, Y. Fu, M. H. Chowdhury, and J. R. Lakowicz, "Metal-enhanced single-molecule fluorescence on silver particle monomer and dimer: coupling effect between metal particles," Nano Lett. **7**(7), 2101–2107 (2007).
27. M. Lessard-Viger, M. Rioux, L. Rainville, and D. Boudreau, "FRET enhancement in multilayer core-shell nanoparticles," Nano Lett. **9**(8), 3066–3071 (2009).
28. V. Komarala, A. L. Bradley, Y. Rakovich, S. Byrne, Y. Gun'ko, and A. Rogach, "Surface plasmon enhanced Forster resonance energy transfer between CdTe quantum dots," Appl. Phys. Lett. **93**(12), 123102 (2008).
29. V. Faessler, C. Hrelescu, A. A. Lutich, L. Osinkina, S. Mayilo, F. Jackel, and J. Feldmann, "Accelerating fluorescence resonance energy transfer with plasmonic nanoresonators," Chem. Phys. Lett. **508**(1-3), 67–70 (2011).
30. M. Lunz, V. A. Gerard, Y. K. Gun'ko, V. Lesnyak, N. Gaponik, A. S. Susha, A. L. Rogach, and A. L. Bradley, "Surface plasmon enhanced energy transfer between donor and acceptor CdTe nanocrystal quantum dot monolayers," Nano Lett. **11**(8), 3341–3345 (2011).
31. X. Zhang, C. A. Marocico, M. Lunz, V. A. Gerard, Y. K. Gun'ko, V. Lesnyak, N. Gaponik, A. S. Susha, A. L. Rogach, and A. L. Bradley, "Experimental and theoretical investigation of the distance dependence of localized surface plasmon coupled Förster resonance energy transfer," ACS Nano **8**(2), 1273–1283 (2014).
32. P. Andrew and W. L. Barnes, "Energy transfer across a metal film mediated by surface plasmon polaritons," Science **306**(5698), 1002–1005 (2004).
33. X. Zhao, P. Wang, and B. Li, "Surface plasmon enhanced energy transfer in metal-semiconductor hybrid nanostructures," Nanoscale **3**(8), 3056–3059 (2011).
34. T. Ozel, P. L. Hernandez-Martinez, E. Mutlugun, O. Akin, S. Nizamoglu, I. O. Ozel, Q. Zhang, Q. Xiong, and H. V. Demir, "Observation of selective plasmon-exciton coupling in nonradiative energy transfer: donor-selective versus acceptor-selective plexcitons," Nano Lett. **13**(7), 3065–3072 (2013).
35. S. Kos, M. Ackermann, V. I. Klimov, and D. L. Smith, "Different regimes of Förster-type energy transfer between epitaxial quantum well and a proximal monolayer of semiconductor nanocystals," Phys. Rev. B **71**(20), 205309 (2005).
36. Y. Li, R. Zhang, Z. Xie, B. Liu, P. Chen, G. Zhang, T. Tao, Z. Zhuang, L. Zhi, T. Gan, and Y. Zheng, "Investigation of surface plasmon coupling with the quantum well for reducing efficiency droop in GaN-based light emitting diodes," J. Appl. Phys. **114**(11), 113104 (2013).

#228319 - $15.00 USD Received 20 Nov 2014; revised 19 Dec 2014; accepted 25 Dec 2014; published 20 Jan 2015

37. S. M. Sadeghi, B. Hood, A. Nejat, R. G. West, and A. Hatef, "Excitation intensity dependence of plasmonic enhancement of energy transfer between quantum dots," J. Phys. D Appl. Phys. **47**(16), 165302 (2014).
38. E. D. Palik, *Handbook of Optical Constants of Solids* (Academic Press, 1985).
39. J. Lee, C. Chiu, C. C. Ke, P. C. Lin, T. Lu, H. Kuo, and S. Wang, "Study of the excitation power dependent internal quantum efficiency in InGaN/GaN LEDs grown on patterned sapphire substrate," IEEE J. Sel. Top. Quantum Electron. **15**(4), 1137–1143 (2009).
40. H. N. Wang, Z. W. Ji, S. Qu, G. Wang, Y. Z. Jiang, B. L. Liu, X. G. Xu, and H. Mino, "Influence of excitation power and temperature on photoluminescence in InGaN/GaN multiple quantum wells," Opt. Express **20**(4), 3932–3940 (2012).
41. T. L. Jennings, M. P. Singh, and G. F. Strouse, "Fluorescent lifetime quenching near d = 1.5 nm gold nanoparticles: probing NSET validity," J. Am. Chem. Soc. **128**(16), 5462–5467 (2006).
42. X. Zhang, C. A. Marocico, M. Lunz, V. A. Gerard, Y. K. Gun'ko, V. Lesnyak, N. Gaponik, A. S. Susha, A. L. Rogach, and A. L. Bradley, "Wavelength, concentration, and distance dependence of nonradiative energy transfer to a plane of gold nanoparticles," ACS Nano **6**(10), 9283–9290 (2012).
43. M. Sukharev, N. Freifeld, and A. Nitzan, "Numerical calculations of radiative and non-radiative relaxation of molecules near metal particles," J. Phys. Chem. C **118**(20), 10545–10551 (2014).

1. Introduction

The development and optimization of high-efficiency semiconductor light emitting diodes (LEDs) for applications in solid-state lighting (SSL) and displays is an area that has received a great deal of attention in recent years. White light generation is typically achieved using phosphor coatings on top of a blue or UV emitting LED [1]. The phosphor coating absorbs some of the light emitted by the LED quantum wells (QWs) and subsequently re-emits light at a higher wavelength. The mixing of the light emitted from the LED and the phosphors results in white light generation. Some of the drawbacks of phosphors include emission in the far-red part of the spectrum, poor color rendering and scattering [2]. Inorganic nanocrystal quantum dots (QDs) are intensively investigated as an alternative to phosphors. Energy transfer from the LED QWs to the nanocrystals can be achieved either through radiative pumping, as for the phosphor coatings [2,3], or via a nonradiative energy transfer mechanism such as Förster resonance energy transfer (FRET) [4,5]. FRET occurs through the near-field Coulomb interaction of a resonant donor-acceptor dipole pair [6]. Radiative pumping is the most commonly used energy transfer mechanism even though FRET has the potential to be more efficient [4,7]. Radiative pumping involves many steps; emission of the photon, extraction of the photon from the LED and reabsorption of the photon. Losses occur, for example, due to limited photon extraction and light scattering. Strategies to efficiently extract photons from LEDs have been a topic of considerable research [8,9]. Nonradiative energy transfer does not require the emission and extraction of the photons but rather the energy is transferred directly to the QDs. A significant drawback for FRET-based devices is its strong dependence on the separation between the donor and acceptor, showing an r^{-6} dependence with a characteristic distance of typically less than ten nanometers. Therefore, implementation of FRET for color conversion in LEDs requires small separations between the donor QWs and QD acceptors. Demonstrations of pumping via nonradiative energy transfer have been achieved using near surface QWs and a thin layer of QDs [4,5,7] or etched structures which allow the acceptors to be brought in close proximity to the QW [10,11]. Both options introduce additional fabrication complexity for commercial devices. Nonradiative energy transfer from QWs to light emitting polymers has also been theoretically and experimentally investigated with a view to color conversion applications [12–17]. Again, the need to minimise the separation between the QW donor and organic acceptor is a critical issue for commercial device fabrication.

In recent times, there have been numerous reports on the use of plasmonic structures, based on both metal nanoparticles and films, to enhance the emission of QWs [18–22] and QDs [23–25]. The enhanced emission can arise due to increased absorption under optical pumping, increased radiative recombination rates and/or scattering by the plasmonic nanostructures. The enhanced local field generated by the plasmonic structures has also been shown to facilitate plasmon-enhanced nonradiative energy transfer. This has been

#228319 - $15.00 USD Received 20 Nov 2014; revised 19 Dec 2014; accepted 25 Dec 2014; published 20 Jan 2015

demonstrated in a variety of material systems and geometries, with reported enhancements of the nonradiative energy transfer distance, rate and efficiency [26–33]. The possibility to achieve higher energy transfer efficiencies over larger distances allows for nonradiative pumping of a larger volume of QDs, and can potentially be exploited to improve the efficiency of nonradiatively pumped down-conversion for white LEDs. To date there has been no investigation of plasmon-enhanced nonradiative energy transfer from a QW donor. In this paper we report on the use of an array of Ag nanoboxes, fabricated using helium-ion lithography (HIL), on an InGaN/GaN QW to enable localised surface plasmon (LSP)-enhanced nonradiative energy transfer to a ~80 nm layer of CdSe/ZnS QDs. The thickness of the QD acceptor layer and the dimensions of the Ag nanoboxes (100 nm x100 nm x 40 nm) are large compared with previous reports of plasmon-coupled nonradiative energy transfer [30,34]. Secondly, there has been no report on the carrier density dependence of the plasmon-coupled nonradiative energy transfer, which is a first step towards implementation in electrically pumped LEDs. In this paper we investigate if the carrier density dependence of the plasmon-coupled nonradiative energy transfer is determined by the same physics as conventional nonradiative energy transfer. FRET from QWs to QDs is known to strongly depend on the QW excitations, excitons or unbound electron-hole pairs [35]. There are some factors which may influence the plasmon-coupled nonradiative energy transfer efficiency. When a plasmonic element is introduced, it can influence the carrier density dependence of the QW emission rate and spectral profile. For example, it has been demonstrated that coupling to plasmonic structures can suppress the efficiency droop in QW LEDs. The emission spectrum from the coupled QW-plasmon system may also be modified relative to the bare QW [36]. The strength of the QW-plasmon coupling is reflected in the modified spontaneous emission rate. Plasmon-coupled nonradiative energy transfer is sensitive not only to the spectral overlap of the donor and acceptor with each other, but also with the spectrum of the plasmon mode [30, 37]. The plasmon-coupled nonradiative energy transfer efficiency is determined by the interplay between the QW spontaneous emission rate, the rate of nonradiative energy transfer to the plasmonic structure and the rate of plasmon-coupled nonradiative energy transfer to the acceptors. The plasmon-coupled energy transfer must compete with the non-radiative energy transfer from the QW to the plasmonic structure. In this paper we investigate the carrier density dependence of plasmon-coupled energy transfer efficiency by probing the carrier density dependences of the individual rates and we find that in the system under study, the plasmon-enhanced nonradiative energy transfer efficiency is constant over the full carrier density range. We also show enhancement of the emission of the CdSe/ZnS QDs acceptors embedded in a ~80 nm thick poly(methyl methacrylate) (PMMA) layer on top of the QW structure.

2. Experimental methods

A schematic of the complete structure is shown in Fig. 1(a). A Ag nanobox array has been fabricated on a single InGaN QW structure and, subsequently, covered in a layer of CdSe/ZnS core-shell QDs embedded in a ~80 nm thick layer of PMMA. The single QW structure used in this work was grown by metal-organic vapour phase epitaxy (MOVPE) on a thick GaN layer on a c-plane sapphire substrate. The QW is 2 nm thick InGaN capped with a 3 nm GaN barrier. It has a peak emission wavelength of 516 nm, Fig. 1(b). The thin top barrier GaN layer was selected to allow for strong near field coupling between the QW and the plasmonic nanoparticles.

A Ag nanobox array was fabricated on top of the GaN barrier using Helium-Ion Lithography (HIL) and a standard lift-off procedure. A 100 nm thick layer of PMMA was first spun onto our GaN top surface and patterned using a Zeiss Orion Plus helium-ion microscope (HIM). After the development of the PMMA, a 5 nm thick layer of Ti followed by a 35 nm thick layer of Ag was deposited using a metal evaporation process. The Ag nanobox array was finally created by a lift-off process. The array consists of nanoboxes

#228319 - $15.00 USD Received 20 Nov 2014; revised 19 Dec 2014; accepted 25 Dec 2014; published 20 Jan 2015

arranged in a two-dimensional square lattice with overall dimensions of 52 µm x 52 µm. A HIM micrograph of the array of 100 nm square boxes with 160 nm gap is shown in Fig. 2(a). The image shows that there is a large degree of uniformity across the entire array and that the aspect ratio of each individual unit is well maintained.

The QDs are CdSe/ZnS core-shell nanocrystals with a diameter of 6.3 nm and a peak emission wavelength of 649 nm, shown in Fig. 1(b). The QDs are embedded in PMMA by first adding the QDs in toluene to a 2.5% wt. PMMA (also dissolved in toluene) solution. This mixture is then sonicated to ensure the QDs are thoroughly dispersed. The solution is then spun down onto the QW decorated by the NP array to create a layer of QDs in PMMA. The layer has a QD concentration of $(1.9 \pm 0.1) \times 10^{21}$ m^{-3}. The QD layer thickness has been measured with a Dektac6 profilometer. It is found that the thickness of the PMMA layer is increased by (19 ± 5) nm on the array compared with a (60 ± 5) nm thickness off the array. The deposition of the QD layer completes the hybrid structure.

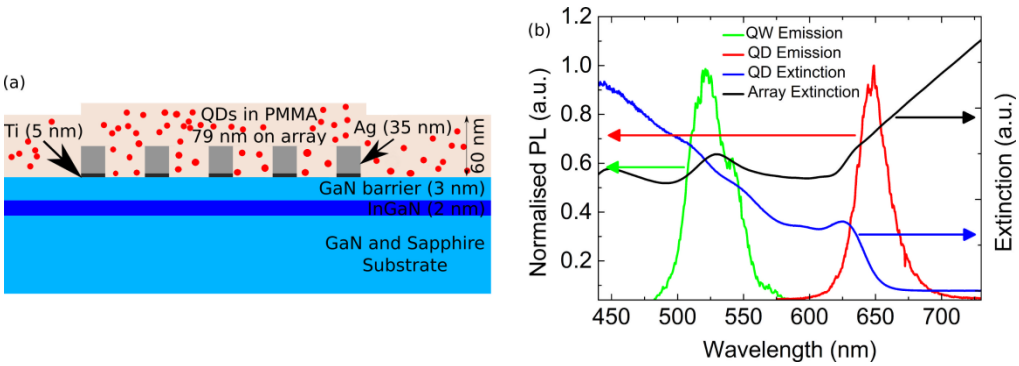

Fig. 1. (a) A schematic of the complete structure (not drawn to scale). (b) The normalized emission spectra of the QW and QDs along with the extinction spectrum of the QDs and the extinction spectrum of the Ag nanobox array.

The emission and energy transfer processes were characterised using photoluminescence (PL) spectroscopy and time-resolved photoluminescence (TRPL). For PL measurements the samples were excited at normal incidence using a pulsed 405 nm laser diode focused using a x40 objective lens. The PL spectra were measured using a fiber-coupled Andor grating spectrometer. The PL decays were measured using a PicoQuant Microtime 200 time-resolved confocal microscope with 150 ps time resolution. The QW or QD emission bands were selected using broad band filters with a full width at half maximum of (70 ± 5) nm centred at 500 nm and 650 nm, respectively. The decay signals and spectra were recorded over an area of 20 µm × 20 µm. All measurements were made at room temperature.

The dimensions and periodicity of the Ag nanoboxes were selected to have overlap of the surface plasmon resonance with the QW donor emission. The nanobox arrays were designed using finite difference time domain commercial software FDTD Solutions from Lumerical Inc. The simulations took account of the PMMA layer on top of the Ag nanoboxes and the 5 nm Ti layer. The dielectric permittivity of the Ag and Ti materials are included using experimentally measured data [38]. The GaN and PMMA layers are modelled with a constant dielectric permittivity of $\varepsilon_{GaN} = 5.35$ and $\varepsilon_{PMMA} = 2.2$, respectively. The extinction spectrum of the Ag nanobox array is simulated using plane-wave excitation. A map of the electric field intensity enhancement due to a dipole source, emitting at 516 nm and placed in the QW below the centre of a nanobox, is shown in Fig. 2(b) and 2(c). The field enhancement is calculated relative to the same layered structure without the Ag nanoboxes. Figure 2(b) and 2(c) show the x-y and x-z maps respectively. It can be seen that for this dipole position the field intensity is enhanced over an extended volume in the vicinity of the Ag nanobox array. It

#228319 - $15.00 USD Received 20 Nov 2014; revised 19 Dec 2014; accepted 25 Dec 2014; published 20 Jan 2015

should be noted that the field intensity enhancement is highly dependent on the position of the dipole source.

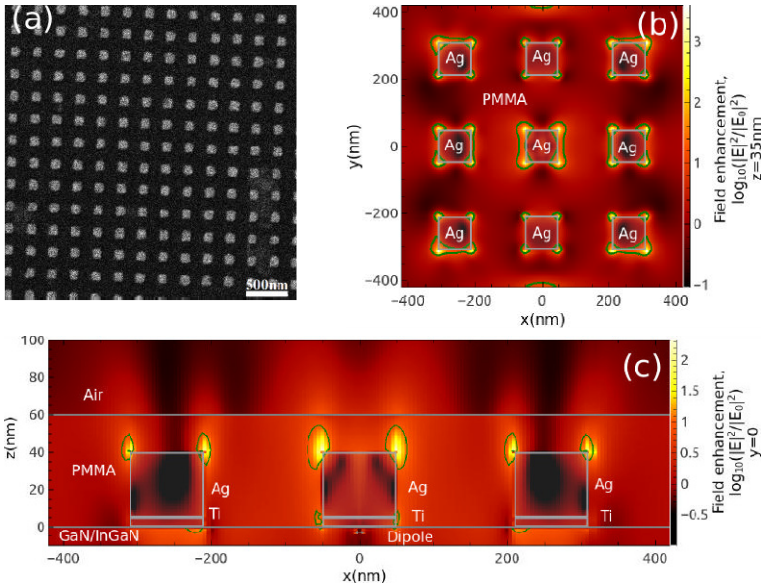

Fig. 2. (a) HIM image of a square array of Ag nanoboxes with 100 nm lateral dimension and 160 nm gap fabricated by HIL on top of the GaN barrier. The field intensity enhancement map in (b) the x-y plane and (c) the x-z plane for a dipole excitation at 516 nm, positioned in the QW layer directly below the Ag nanobox at x = y = 0. The olive line indicates where the field intensity is enhanced by a factor of 10.

3. Results and discussion

The dependence of the QW emission properties are considered first. The calculation of the injected carrier density, n, is given by Eq. (1),

$$n = \frac{P}{(h\nu) * \theta * d_{active} * f} * \left[1 - \exp\left(-\alpha_{InGaN} d_{active}\right)\right] * (1 - R) \quad , \qquad (1)$$

where P is the laser pumping power, $h\nu$ is the energy of the injected photons, θ is the spot size of pumping laser, d_{active} is the thicknesses of the active region, f is the repetition rate of pumping laser, α_{InGaN} is the absorption coefficient of the InGaN QW, and R is the reflectance at the wavelength of the pump laser at 405 nm, respectively [39]. Here the spot diameter is 0.43 µm, d_{active} is 2 nm, f is 10 MHz, α_{InGaN} is 10^4 cm^{-1} and R is 0.15. The PL intensity of the single QW as a function of injected carrier density, n, is shown in Fig. 3(a). The intensity is measured from the PL decay at $t = 0$. At lower carrier densities the PL increases linearly while at higher excitation powers a quadratic dependence is present, which is characteristic of free-carrier recombination. There is some evidence of saturation at the highest carrier densities which may be due to carrier leakage. In the inset of Fig. 3(b) we show the average PL lifetime of the single QW, τ_{QW}, over the same range of injected carrier densities. The PL decay curves are fit with a bi-exponential and the average PL lifetime is given by Eq. (2),

$$\tau_{avg} = \frac{I_1 * \tau_1^2 + I_2 * \tau_2^2}{I_1 * \tau_1 + I_2 * \tau_2} \quad , \qquad (2)$$

where I_1 and I_2 are the intensity amplitudes for the exponential decays with two different lifetimes τ_1 and τ_2, respectively.

#228319 - $15.00 USD Received 20 Nov 2014; revised 19 Dec 2014; accepted 25 Dec 2014; published 20 Jan 2015

It can be seen that in the lower carrier density range, up to approximately $1x10^{18}$ cm^{-3}, the lifetime increases. This is attributed to the presence of defect related nonradiative recombination centres [40]. At higher carrier densities these defect states become saturated and the average lifetime begins to decrease as the excitation intensity is further increased. In this range the radiative recombination processes dominate. We concentrate on the higher carrier density range from $1x10^{18}$ cm^{-3} to $2x10^{19}$ cm^{-3} from this point forward.

Figure 3(b) shows the spontaneous emission rate of the QW as a function of injected carrier density with and without the addition of the QDs in the absence of the Ag nanobox array, τ_{QW}^{-1} and τ_{QW-QD}^{-1}, respectively. The introduction of the QDs has no measurable effect on the QW PL decay rate indicating that there is insignificant direct nonradiative energy transfer from the QW to the QD layer in the absence of the plasmonic nanostructures. It should be noted that for all measurements, of the bare QW and the nanobox decorated QW, there is a layer of PMMA deposited on top to facilitate direct comparison of the QW PL lifetime with the structures having QDs embedded in the PMMA host layer.

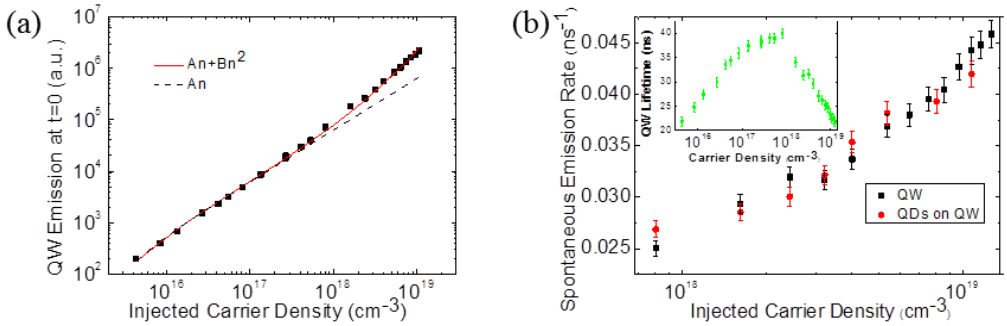

Fig. 3. (a) The QW emission at t = 0 as a function of injected carrier density. (b). The spontaneous emission rate of the QW with (red circles) and without (black squares) QDs as a function of injected carrier density. Inset: The average QW PL lifetime as a function of injected carrier density.

Next we focus on the interaction of the QW and QDs with the Ag nanobox array. Figure 4(a) shows the PL decays of the bare QW, the QW with the Ag nanobox array deposited on top, and the completed structure with the QD layer. The decays were recorded at an injected carrier density of $5.4x10^{18}$ cm^{-3}. It is noted that the QW PL lifetime and emission are dramatically reduced due to the presence of the Ag nanobox array. They are further reduced by the addition of the QDs. Considering, firstly, the effect of the Ag nanobox array on the QW emission, the reduction in PL lifetime and emission signifies a quenching process due to nonradiative energy transfer from the QW to the metal nanoparticles. Emission quenching by energy transfer to metal nanoparticles has been extensively reported by the literature [41–43]. This can be quantified as a quenching efficiency, E_Q, which is given by Eq. (3),

$$E_Q = 1 - \frac{\tau_{QW-NB}}{\tau_{QW}} \tag{3}$$

where $\tau_{QW} = (27 \pm 2)$ ns is the average PL lifetime measured for the bare QW and $\tau_{QW-NB} = (3.5 \pm 0.2)$ ns is the average PL lifetime for the QW decorated with the Ag nanobox array. The quenching is (90 ± 10)% indicating a very strong interaction between the QW and Ag nanoboxes. The further reduction of the QW lifetime and emission after the addition of the QDs indicates the presence of Förster-like nonradiative energy transfer from the QW to the QDs. This is evidence for LSP enhancement of the nonradiative energy transfer process mediated by the Ag nanoboxes since, as noted earlier, in the absence of the Ag nanobox array

#228319 - $15.00 USD Received 20 Nov 2014; revised 19 Dec 2014; accepted 25 Dec 2014; published 20 Jan 2015

no measurable signatures of nonradiative energy transfer from the QW to the QDs could be observed. The plasmon-coupled nonradiative energy transfer efficiency, E_{NRET}, is defined by Eq. (4),

$$E_{NRET} = 1 - \frac{\tau_{QW-NB-QD}}{\tau_{QW-NB}}, \quad (4)$$

where $\tau_{QW-NB-QD} = (2.6 \pm 0.2)$ ns is the QW PL lifetime after the addition of the QD layer. For the example shown in Fig. 4(a) a plasmon-enhanced nonradiative energy transfer efficiency of (25 ± 3) % is observed. Figure 4(b) shows the average PL lifetime of the bare QW, the QW decorated with the Ag nanobox array and the QW with both the Ag nanoboxes and QDs, as a function of the injected carrier density. The average lifetime of the QW-Ag nanobox-QD structure is shorter relative to the QW-Ag nanobox structure at all carrier densities.

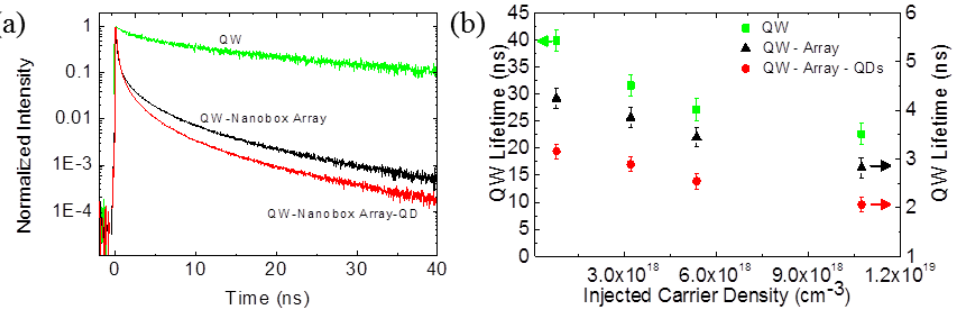

Fig. 4. (a) The normalized PL decays of the bare QW (green line), the QW with nanobox array (black line) and the QW with nanobox array and QD layer (red line) at a carrier density of 5.4×10^{18} cm^{-3}. (b) The average PL lifetime of the bare QW (green squares), the QW with nanobox array (black triangles) and the QW with nanobox array and QD layer (red circles) as a function of injected carrier density.

Figure 5(a) shows the carrier density dependence of the quenching and QW to QD nonradiative energy transfer rates. Both increase with increasing carrier density. As previously reported the carrier density dependence of the Förster nonradiative energy transfer rate from a QW is determined by whether the electronic excitations in the QW are free electrons and holes or bound electron hole pairs (excitons) [4, 35]. For donor QW free carriers the energy transfer rate is proportional to the carrier density, whereas it is independent of carrier density for donor QW excitons. A linear dependence of the direct nonradiative energy transfer rate from an InGaN QW to a monolayer of CdSe QDs has been experimentally reported and found to be in good agreement with a theoretical model for free carrier QW excitations [35]. The QW PL quenching by the Ag nanobox array is also considered to arise due to nonradiative energy transfer to the metal nanoparticle acceptors. The observed linear dependence of the quenching rate on the carrier density therefore suggests nonradiative energy transfer from free carrier excitations in the donor QW. This is consistent with the earlier analysis of the QW emission properties, presented in Fig. 3, which showed evidence of free carrier recombination in this carrier density range. The plasmon-coupled nonradiative energy transfer from the QW to the QDs indicates a similar behaviour, though it is noted that the errors on the measured rates in this case are larger due to smaller lifetimes (see Fig. 4(b)). The QW excitations are the donors for both nonradiative energy transfer to the metal nanoparticles and to the QDs, therefore, a similar carrier density dependence might be expected for both cases. However, further evidence for the trend of the plasmon-coupled energy transfer rate can be obtained by looking at the energy transfer efficiency and this will be discussed below.

#228319 - $15.00 USD Received 20 Nov 2014; revised 19 Dec 2014; accepted 25 Dec 2014; published 20 Jan 2015

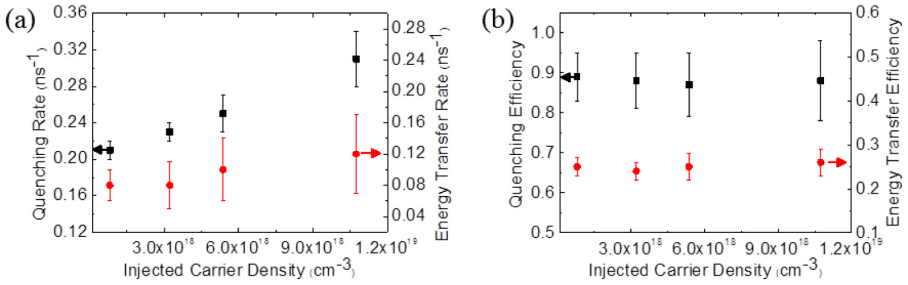

Fig. 5. (a). The QW emission quenching rate (black squares) and the plasmon-coupled nonradiative energy transfer rate (red circles) as a function of the injected carrier density. (b) Quenching efficiency (black squares) and plasmon-coupled nonradiative energy transfer efficiency (red circles) as a function of injected carrier density.

The quenching efficiency, E_Q, and plasmon-coupled QW to QD nonradiative energy transfer efficiency, E_{NRET}, were calculated from the QW lifetimes using Eqs. (3) and (4). Both efficiencies are found to be independent of the injected carrier density, as seen in Fig. 5(b). The quenching efficiency is approximately 90% across the full carrier density range, while the plasmon-coupled QW to QD nonradiative energy transfer has an efficiency of approximately 25%. The nonradiative energy transfer efficiency can also be expressed as

$$E_{NRET} = \frac{k_{NRET}}{k_{QW} + k_{QW-NB} + k_{NRET}} \quad , \tag{5}$$

where k_{QW} is the spontaneous emission decay rate for the bare QW, k_{QW-NB} is the QW quenching rate for the QW decorated with the Ag nanobox array and k_{NRET} is the plasmon-coupled QW to QD nonradiative energy transfer rate. The observation of a carrier density independent energy transfer efficiency confirms that k_{NRET} must be increasing to compete with the increasing QW spontaneous emission and quenching rates, k_{QW} and k_{QW-NB} shown in Figs. 3(b) and 5(a), respectively.

There are a number of aspects of this process that are noteworthy. Firstly, the Ag nanobox array provides a sufficiently large local electromagnetic field to allow for a nonradiative energy transfer path between the QW and QDs that is otherwise too weak to measure in the absence of the plasmonic nanostructures. Secondly, the plasmon-enhanced nonradiative energy transfer rate is sufficiently fast to compete with the efficient QW quenching across the full carrier density range. Thirdly, the increase in the nonradiative energy transfer efficiency indicates an increase in the distance over which the energy transfer occurs. The conventional nonradiative energy transfer efficiency can be written as $\left(1+\frac{r^n}{R_0^n}\right)^{-1}$ where r is the separation between the donor and acceptor dipoles, R_0 is the characteristic distance at which the energy transfer efficiency is 50% and the exponent n depends on the geometry. For example, for nonradiative energy transfer between two point dipoles n = 6, from a point dipole to a plane of acceptors n = 4 and for nonradiative energy transfer between two planes n = 2. Therefore, the increase in the nonradiative energy transfer efficiency can be expressed as a plasmon-enhanced R_0. Finally, the plasmon-enhanced nonradiative energy transfer is found to have the same dependence on carrier density as conventional Förster-like energy transfer from QW free carriers excitations to colloidal QDs in the absence of the plasmonic structures.

Up to this point we have focussed on the properties of the plasmon-coupled energy transfer in this hybrid system extracted from the changes in the QW lifetime, however, there

#228319 - $15.00 USD Received 20 Nov 2014; revised 19 Dec 2014; accepted 25 Dec 2014; published 20 Jan 2015

is also evidence of the plasmon-coupled energy transfer in the QD emission. Figure 6(a) shows the QD PL decays on and off a Ag nanobox array fabricated on a bulk GaN layer. This allows us to investigate the interaction between the QDs and the Ag nanoboxes with the same excitation source but in the absence of the QW. A (27 ± 3) % reduction in the QD average PL lifetime is observed on the array relative to off the array. Furthermore, Fig. 6(b) shows the QD PL decays both on and off the Ag nanobox array on the QW sample. In this case the QDs on the array show an (12 ± 2) % increase of the PL lifetime relative to QDs off the array. Therefore, the influence of the plasmon-enhanced energy transfer is sufficiently strong that the QD PL lifetime not only recovers from the reduction on the array but is even further increased. The decay over 40 ns is presented in the inset, while the decay over the first 8 ns is given in the main figure to more clearly show the change in the PL decay.

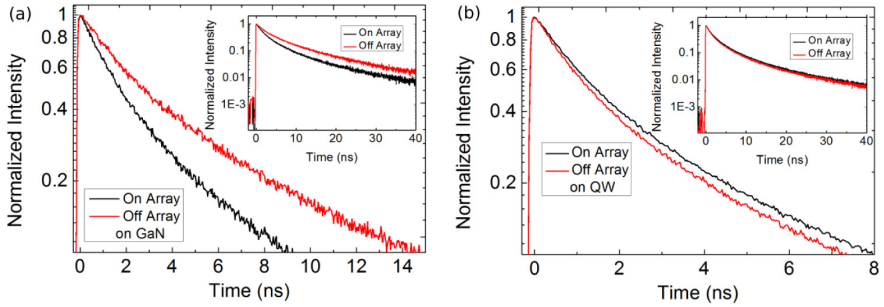

Fig. 6. (a) The QD PL decay on and off the Ag nanobox array on a GaN bulk layer. (b) QD PL decay on and off of Ag nanobox array on the QW sample. The insets shows the PL decays over 40 ns.

The PL spectra for the QW and QDs, with and without the Ag nanobox array, are shown in Fig. 7. Firstly, from the PL spectra for the bare QW and the QW with the QDs in the absence of the Ag nanobox array it is clear that the presence of the QDs alone have little influence on the QW emission. The influence of the nanobox array on the QD emission is observed in the PL spectrum for the QDs on the Ag nanobox array on the bulk GaN layer. The direct interaction between the Ag nanoboxes and the QDs results in quenching of the QD emission by (11 ± 4)%. This reduction in QD emission is also confirmed by integrating the TRPL decays for the QDs on and off the array on the bulk GaN layer. As discussed earlier the QW emission is highly quenched by the Ag nanobox array.

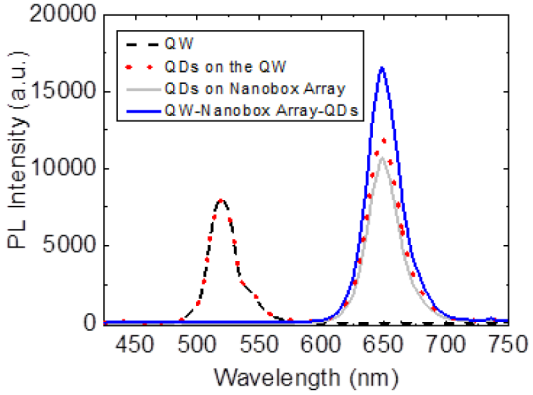

Fig. 7. PL spectra of the bare QW (dashed black line), QDs on the QW (red dotted line), QDs on the Ag nanobox array on the bulk GaN layer (grey line), and complete QW-Ag nanobox-QD system (blue solid line).

#228319 - $15.00 USD Received 20 Nov 2014; revised 19 Dec 2014; accepted 25 Dec 2014; published 20 Jan 2015

Finally, when we look at the PL spectrum of the complete QW-Ag nanobox-QD structure, it can be seen that the QW emission is effectively completely quenched and that the QD emission not only recovers from the direct quenching by the Ag nanobox array but exhibits an emission enhancement of (41 ± 10) % relative to the QW-QD structure. Again, this enhancement of the QD emission is confirmed by integrating the TRPL curves for the QDs on and off the Ag nanobox array on the QW. These QD PL quenching and enhancement factors are measured by direct comparison of the PL on and off the Ag nanobox array. However, taking account of the difference in the PMMA layer thickness on the Ag nanobox array compared with off the array, and the volume filled by the Ag nanoboxes, the corrected QD PL quenching and enhancement are 27% and 16%, respectively. It is noted that the plasmon-coupled nonradiative energy transfer has compensated for the direct quenching of the QD PL by the Ag nanobox array to yield an overall enhancement of the QD layer emission. Comparing the emission from the QDs on the nanobox array with the QD emission in the full structure (spectra shown in Fig. 7) shows that the enhancement due to the plasmon-coupled energy transfer mechanism alone is 58%.

4. Summary

In conclusion, we have investigated plasmon-enhanced nonradiative energy transfer from an InGaN/GaN SQW to core-shell CdSe/ZnS QDs embedded in a ~80 nm host PMMA layer. The plasmonic structure is a Ag nanobox array fabricated by HIL and designed such that the QW emission peak spectrally overlaps with the LSP resonance. Both the QW emission quenching rate and the plasmon-coupled nonradiative energy transfer rate were found to increase with increasing QW carrier density. The quenching and energy transfer efficiencies were carrier density independent. A quenching efficiency of 90% of the QW emission by the Ag nanobox array and a QW to the QD plasmon-enhanced energy transfer efficiency of 25% were observed. Despite strong direct quenching by the metal nanoparticles, the plasmon-coupled energy transfer results in a 16% increase of the QD emission. Further optimization of the properties of the nanobox array and the QD layer thickness would yield higher enhancement of the QD emission. The carrier density dependence of the nonradiative energy transfer from the QW to the Ag nanobox array and that of the plasmon-enhanced nonradiative energy transfer from the QW to the QD layer are found to be the same as for conventional Förster-like energy transfer. This indicates that secondary effects of the plasmon coupling, such as spectral shifts, do not have a significant effect in the system studied. Plasmon-coupled nonradiative energy transfer may alleviate some of the constraints on the use of nonradiative pumping for down-conversion based LEDs, such as the need for very thin QD layers or etching of the QW structures.

Acknowledgments

This work was supported by Science Foundation Ireland (SFI) under grant number 10/IN.1/12975 and the National Access Programme Grant under grant number NAP 338, and enabled using facilities funded by Irish Higher Education Authority Programme for Research in Third Level Institutions Cycles 4 and 5 via the INSPIRE and TYFFANI projects. We also acknowledge the Advanced Microscopy Laboratory (AML) for use of the helium-ion microscope. TCS acknowledges a postdoctoral research fellowship from the Irish Research Council and PJP a SFI Engineering Professorship (SFI/07/ EN/E001A).

#228319 - $15.00 USD Received 20 Nov 2014; revised 19 Dec 2014; accepted 25 Dec 2014; published 20 Jan 2015